Characteristics of the Flank Magnetopause: MMS Results

J. Burch, H. Hietala, J. P. Eastwood, C. Norgren, B. Lavraud, P. Tenfjord, S. Fadanelli, K. J. Trattner, S. Eriksson, V. Constantinescu, et al.

JGR Space Physics

RESEARCH ARTICLE
10.1029/2019JA027623

Characteristics of the Flank Magnetopause: MMS Results

S. Haaland[1,2], G. Paschmann[3], M. Øieroset[4], T. Phan[4], H. Hasegawa[5], S. A. Fuselier[6,7], V. Constantinescu[8], S. Eriksson[9], K. J. Trattner[9], S. Fadanelli[10,11], P. Tenfjord[12], B. Lavraud[10], C. Norgren[12], J. P. Eastwood[13], H. Hietala[13], and J. Burch[6]

[1]Max-Planck Institute for Solar Systems Research, Göttingen, Germany, [2]Birkeland Centre for Space Science, University of Bergen, Bergen, Norway, [3]Max-Planck Institute for Extraterrestrial Physics, Garching, Germany, [4]Space Sciences Laboratory, University of California, Berkeley, CA, USA, [5]Institute of Space and Aeronautical Science, Aerospace Exploration Agency, Sagamihara, Japan, [6]Southwest Research Institute, San Antonio, TX, USA, [7]Department of Physics and Astronomy, University of Texas at San Antonio, San Antonio, TX, USA, [8]Institute of Space Science, Bucharest, Romania, [9]Laboratory for Atmospheric and Space Physics, University of Colorado Boulder, Boulder, CO, USA, [10]Institut de Recherche en Astrophysique et Planétologie, CNRS, UPS, CNES, Université de Toulouse, Toulouse, France, [11]Dipartimento di Fisica, Università di Pisa, Pisa, Italy, [12]Space Plasma Physics Group, University of Bergen, Bergen, Norway, [13]Blackett Laboratory, Imperial College London, London, UK

Abstract We have used a large number of magnetopause crossings by the Magnetospheric Multiscale (MMS) mission to investigate macroscopic properties of this current sheet, with emphasis on the flanks of the magnetopause. Macroscopic features such as thickness, location, and motion of the magnetopause were calculated as a function of local time sector. The results show that the flanks of the magnetopause are significantly thicker than the dayside magnetopause. Thicknesses vary from about 650 km near noon to over 1,000 km near the terminator. Current densities vary in a similar manner, with average current densities around noon almost twice as high as near the terminator. We also find a dawn-dusk asymmetry in many of the macroscopic parameters; the dawn magnetopause is thicker than at dusk, while the dusk flank is more dynamic, with a higher average normal velocity.

Key Points:
- The magnetopause flanks are characterized using MMS observations
- Magnetopause flanks are thicker and have lower current density than the dayside
- The dawn magnetopause is marginally thicker than at dusk

Correspondence to:
S. Haaland,
Stein.Haaland@uib.no

Citation:
Haaland, S., Paschmann, G., Øieroset, M., Phan, T., Hasegawa, H., Fuselier, S. et al. (2020). Characteristics of the flank magnetopause: MMS results. *Journal of Geophysical Research: Space Physics*, *125*, e2019JA027623. https://doi.org/10.1029/2019JA027623

Received 10 NOV 2019
Accepted 11 JAN 2020
Accepted article online 3 FEB 2020

1. Introduction

The magnetopause is a current sheet separating the magnetosphere with its geomagnetic field on the inside from the shocked solar wind and its embedded interplanetary magnetic field (IMF) on the outside. Due to its importance for the transfer of momentum, mass, and energy, the terrestrial magnetopause has been extensively studied (see reviews in, e.g., Hasegawa, 2012; Paschmann et al., 2005). Most of the attention has been on the subsolar magnetopause, where the interaction between the IMF and geomagnetic field is believed to be strongest.

An interesting property of the terrestrial magnetopause, highlighted in Haaland et al. (2014), is the presence of a persistent dawn-dusk asymmetry in many macroscopic parameters. Using a large collection of magnetopause crossings from the Cluster mission, they found that the dusk flank of the magnetopause was on average thinner, had a higher current density, and had a lower normal velocity than its dawn counterpart. Later, a comparison of the dawn, dusk, and dayside magnetopause, using observations from the THEMIS mission (Haaland et al., 2019), came to similar conclusions: A thinner dusk flank magnetopause current sheet, and a thicker, more dynamic dawn flank magnetopause current sheet. The epoch (2007–2009) as well as the seasonal phasing of the THEMIS orbit were different from the Cluster study, thus eliminating some uncertainties about possible tilt angle dependence and seasonal bias in the Cluster data set.

The high variability of the magnetopause implies that large-scale, persistent asymmetries cannot be derived from single-event studies, or even conjugate studies with one spacecraft at each flank. Such conclusions can only be derived by exploiting large data sets from space missions with the proper instrumentation and with extensive coverage in local time across the magnetopause. The Magnetospheric Multiscale mission (MMS; see Burch et al., 2016) provides a new opportunity for such a study. MMS can measure plasma moments with a much higher time resolution than earlier missions, and the intercalibration between electron and ion detectors enables a direct determination of electric currents from plasma moments.

In the present paper, which is based on discussions between members of an international team of experts hosted by the International Space Science Institute (ISSI) in 2018–2019, we have utilized a large database of MMS burst mode intervals to characterize the flanks of the magnetopause, to compare the dayside magnetopause to the flank magnetopause, and to check whether asymmetries found in the Cluster and THEMIS observations also exist in MMS observations.

The paper is organized as follows. In section 2 we provide a brief description of the data basis and the methodology to calculate key magnetopause parameters. Section 3 shows statistical results based on the MMS data set, and highlights some of the local time asymmetries found. Section 4 discusses the results and compares the findings to the above mentioned Cluster and THEMIS studies. Section 5 summarizes the results.

2. Data and Methodology

The MMS measurements used in the present study stem from a database of approximately 18,000 burst mode intervals from the period September 2015 to April 2018. This database contains characterizations and classifications of current sheets based on measurements from the Fast Plasma Investigation (FPI), described in Pollock et al. (2016), the Fluxgate Magnetometer, described in Russell et al. (2016) and the Hot Plasma Composition Analyzer, described in Young et al. (2016).

2.1. The MMS Current Sheet Database

A detailed description about the collection, processing, and ingestion of MMS burst mode data into a large current sheet database is already given in Paschmann et al. (2018). The initial version of the MMS current sheet database covered Phase I of the MMS mission (September 2015 to April 2017). As a follow-up to this effort, an ISSI team was established to utilize and perform further analysis of the data set. In particular, the database was extended to include data from Phase II of the MMS mission (September 2017 to April 2018). Also, almost all current sheet crossing events in the database were visually inspected and manually classified and characterized by the four lead authors of this paper. The classification scheme is outlined in Appendix A.

Since the prime objective of the MMS mission is to resolve small scale details of the diffusion regions in reconnection sites, the four MMS spacecraft fly in close formation, with separation distances sometimes as small as 7 km. For a study of macroscopic properties and asymmetries like the present one, having four closely located spacecraft does not bring any significant advantages compared to having observations from just one spacecraft, especially since the MMS plasma instruments can provide accurate current density measurements (Lavraud et al., 2016; Phan et al., 2016). Following recommendations from the instrument teams and the MMS principal investigator, all results in the present study are therefore based on measurements from the MMS Spacecraft 2. The previous MMS current sheet database and its characterizations in Paschmann et al. (2018) were based on MMS Spacecraft 1.

The Paschmann et al. (2018) study focused on macroscopic features of the dayside magnetopause, and discarded crossings where $|Ygse| > 10$. The extension of the database to cover Phase II of the MMS mission brought a number of additional flank crossings, and has enabled a dedicated dawn-dusk study and a comparison of the dayside and flank magnetopause. MMS traverses the dawn flank of the magnetopause during February to April and the dusk flank around September to October. Figure 1 shows the location of crossings included in the present study. For comparison, we also show the corresponding coverage of the earlier Cluster study described in Haaland et al. (2014) (containing flank magnetopause crossings during the years 2001–2010) and THEMIS study described in Haaland et al. (2019) (magnetopause traversals during 2007–2009).

We note that the spatial coverage between the three missions only partially overlaps. For MMS, the 12 Re apogee during Phase I means that relatively few flank crossings near the terminator were observed, as the nominal magnetopause position near the terminator is further away. Consequently, MMS flank crossings from this period are somewhat biased toward periods with high solar wind dynamic pressure enabling the magnetopause to move closer to Earth. Phase II of the MMS mission (apogee raised to 25 Re), provided more flank crossings, but the focus was shifted to nightside tail reconnection observations. For comparison, Cluster, with its 19 Re apogee and polar orbit, skimmed the flank magnetopause behind the terminator over several months each year, and usually crossed the magnetopause at high latitudes. The Haaland et al. (2014)

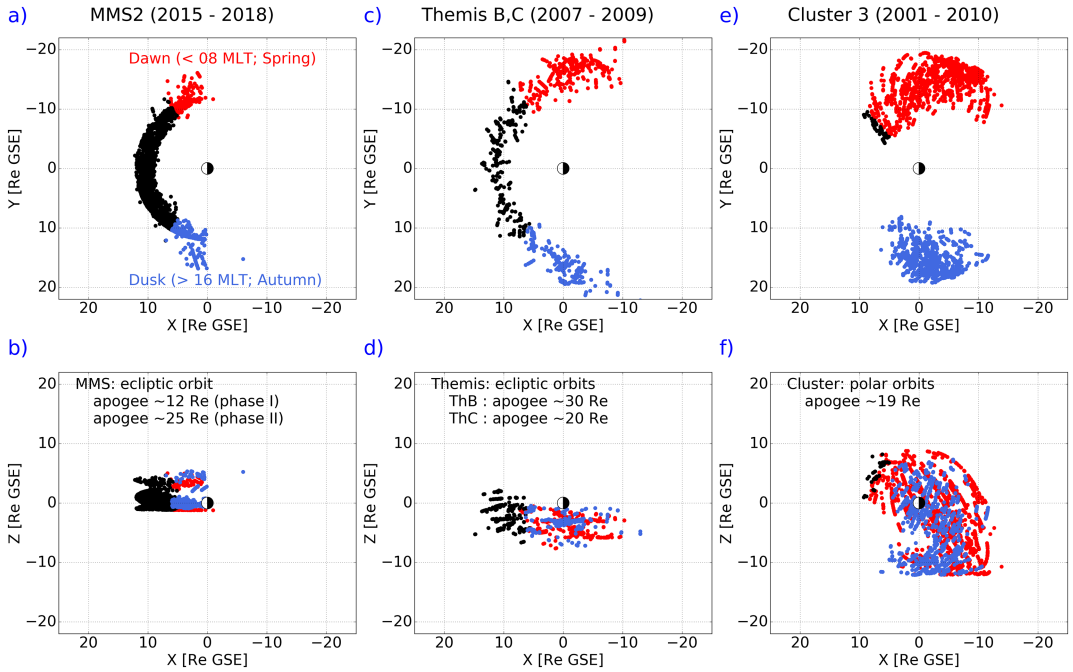

Figure 1. (a, b): XY_{GSE} and XZ_{GSE} projections of the positions of magnetopause crossing positions used in this study. Black dots indicate dayside crossings, that is, crossings within a magnetic local time (MLT) sector between 08 and 16. Blue symbols show crossings in MLT sectors beyond 16 (traversed by MMS around September–October). Red symbols show dawn crossings in MLT sectors earlier than 08 (traversed by MMS around February to April). (c and d) The same positions and projections, but for the THEMIS study in Haaland et al. (2019). (f and g) The crossing positions from the Cluster study of Haaland et al. (2014). Note that Cluster has a polar orbit, but only crossings at GSE latitudes below 45° were characterized.

study only used Cluster crossings below 45° GSE latitude to characterize the magnetopause flanks. THEMIS and MMS on the other hand both have near ecliptic orbit and thus cross the magnetopause at low latitudes.

2.2. Method to Derive Macroscopic Magnetopause Parameters

The procedure to calculate magnetopause thickness, velocity, and current density is identical to that of Paschmann et al. (2018). With exception of current density calculations, the methodology is also very similar to the methodology used in the Cluster and THEMIS dawn-dusk studies described in Haaland et al. (2014) and Haaland et al. (2019). Below, we give a brief overview of the method and show an example of the definitions used in this paper.

2.2.1. Crossing Time and Duration

Magnetopause crossing times and durations of the traversals are based on a one-dimensional Harris sheet approach (Harris, 1962), in which the current sheet thickness is defined by a 76% change in the L component of the magnetic field. The LMN coordinate system is determined from a minimum variance analysis of the magnetic field over the full burst interval. Experience has shown that the L component (maximum variance component) is usually well defined and not very sensitive to the length of the analysis interval.

As explained in Paschmann et al. (2018), the determination of crossing time and duration is based on a 5 s boxcar averaged magnetic field. We define the current sheet crossing time as the midpoint (50% level) of the full B_L transition, and the duration, t_{CS}, as the interval where the magnetic field changes from 12% to 88% of its asymptotic values, as illustrated in Figure 2a).

With knowledge about the magnetopause normal velocity (see section 2.2.2), the thickness of the magnetopause can be calculated. In addition to expressing the thickness in units of kilometers, it is often useful to normalize the thickness to universal physical units like ion inertial length or ion gyroradius. The former is a characteristic scale at which ions become demagnetized. The ion inertial length is given by

$$\lambda_i \text{ (km)} = \sqrt{\frac{m_i}{n_i q^2 \mu_0}} \simeq 222/\sqrt{n_i}, \quad (1)$$

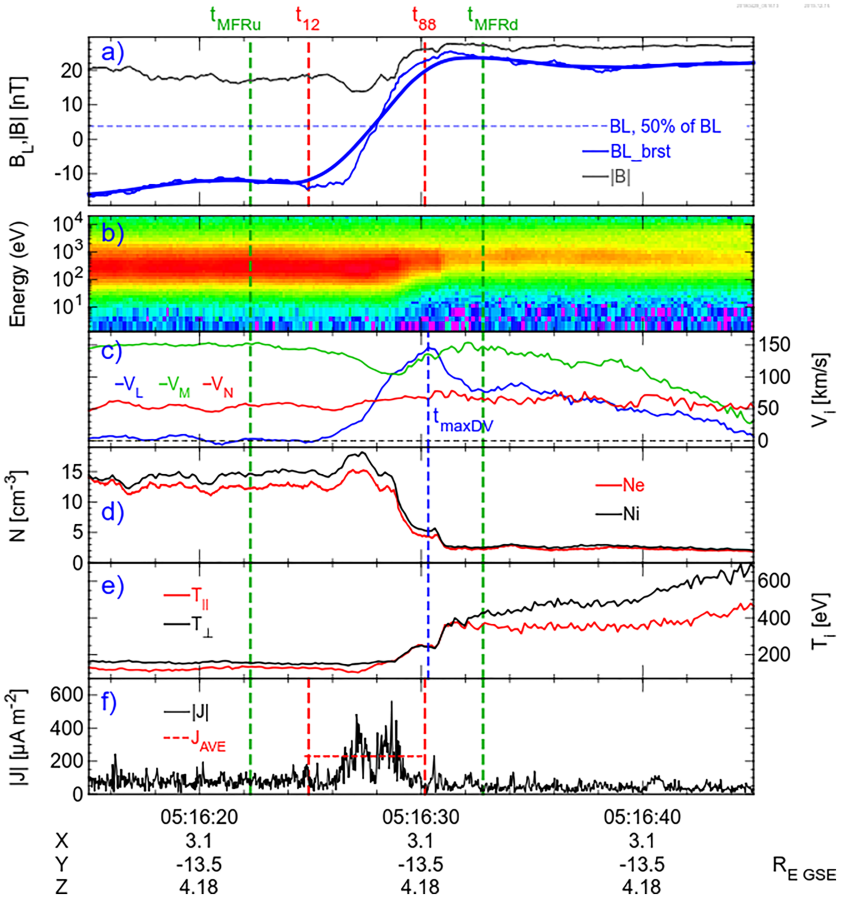

Figure 2. Example of measurements taken during an MMS crossing of the dawn flank magnetopause. MMS spacecraft 2 traversed the magnetopause near [3.1, −13.5, 4.2] Re_{GSE} (MLT = 6.9), at about 05:16 UT on 29 April 2018. (a) Magnitude of the B field (gray line) and the B_L component of the magnetic field (blue lines). We use the smoothed version of B_L (blue heavy line) to define the crossing time and duration. (b) Ion spectrogram from the FPI instrument. (c) Bulk flow velocity in LMN coordinates. (d) FPI ion and electron density. (e) Parallel and perpendicular ion temperature from FPI. (f) Current density, derived from FPI moments. The horizontal dashed red line shows J_{AVE}—the *average* current density across the current sheet. The horizontal blue dashed line in panel (a) marks where the 50% level of B_L is reached. The intersection of this line with the smoothed B_L defines the crossing time, t_0. Vertical red lines in panels (a) and (f) indicate the current sheet duration, $t_{cs} = t_{12}$ to t_{88} used to determine the current sheet thickness. Vertical green lines indicate the time interval used to calculate the magnetopause normal velocity, $t_{MFR} = t_{MFRu}$ to t_{MFRd}, where the subscripts refer to upstream (magnetosheath) and downstream (magnetosphere), respectively. The vertical blue line in panels (c) to (e) indicates where $\Delta V = V_{MFRu} - V$ maximizes (see section 2.2.4).

and the ion gyroradius is given by

$$R_{gi}\ (\mathrm{km}) = \frac{m_i v_{i\perp}}{qB} \quad \simeq \quad 140\sqrt{T_{i\perp}}/B, \tag{2}$$

where m_i is the ion mass, q is the elementary charge, B is the magnetic field, μ_0 is the magnetic permeability of vacuum and $T_{i\perp}$ is the perpendicular ion temperature. The right part of these two equations are simplifications assuming that all ions are protons, and that the magnetic field is given in units of nanotesla, the density in units of per cubic centimeter, and the temperature in units of electron volts. In our calculations we normalize to these physical units using the upstream (magnetosheath) values of B, n_i, and $T_{i\perp}$.

For the example in Figure 2, the current sheet crossing duration, t_{CS}, is only around 5 s, and the normal velocity about 81 km/s. The calculated thickness is then approximately 410 km, corresponding to 4 R_{gi} or about 7 λ_i. For this particular event, which has a very short duration, one could argue that real transition in B_L is even faster, and that the 5 s boxcar filter in the Paschmann et al. (2018) procedure leads to an overestimation of the thickness. The boxcar averaging improves the automated detection and characterization

of current sheets and eliminates the effect of fluctuations caused by motion or small scale structures inside the main current sheet. We emphasize that the 5 s boxcar averaging is only used to determine crossing time and duration—all other parameters and calculations use high-resolution B field measurements.

2.2.2. Magnetopause Normal Velocity

The magnetopause velocity is determined from the Minimum Faraday Residue (MFR) analysis of the electric field (Khrabrov & Sonnerup, 1998b; Sonnerup et al., 2008; Terasawa et al., 1996). MFR returns the frame of reference which minimizes the tangential electric field and thus represents the convective motion of the magnetopause as a coherent structure. MFR analysis involves a least squares minimization scheme and provides a set of eigenvalues that are used to assess the quality of the frame determination as well as a set of eigenvectors that are used to estimate the orientation (and thus the boundary normal, $\vec{n}$) of the magnetopause.

As in Paschmann et al. (2018) and Haaland et al. (2019), we also perform a complimentary deHoffmann-Teller (HT) analysis (Khrabrov & Sonnerup, 1998a; Paschmann & Sonnerup, 2008). To get the normal velocity from HT analysis, the frame velocity is projected along the boundary normal, $\mathbf{n}$, obtained from a constrained minimum variance of the magnetic field (MVAB0; see Sonnerup & Scheible, 1998).

Since our model of the magnetopause is that of a near one-dimensional MHD structure, assumed to be time invariant during the crossing interval, any kinetic effects are neglected, and the electric field used in the above methods are derived from the magnetic field and ion bulk velocity, that is, $\mathbf{E} = -\mathbf{V}_i \times \mathbf{B}$.

The MFR, HT, and MVAB0 analyses all use measurements from a time interval, $t_{MFR} = |t_{MFRu} - t_{MFRd}|$ (where the subscripts u and d refer to upstream and downstream), which is twice the duration of the actual current sheet duration, t_{cs}. In Figure 2, this interval is indicated by vertical green lines. The consistency between the MFR and HT velocities, as well as eigenvalues of the analyses are used to assess the quality of the velocity calculation.

An important advantage of the MMS mission compared to Cluster and THEMIS is the high time resolution of the plasma data. For the above calculations, we require a minimum of five plasma samples. For Cluster and THEMIS, this corresponds to a minimum of 20 and 15 s, respectively, or about 400–600 km using the average magnetopause velocities from those spacecraft. The FPI plasma instruments on board MMS have cadences of 150 ms (ions) and 30 ms (electrons), respectively, and thus enable resolving structures with scales sizes of a few kilometers. Indeed, as shown in Paschmann et al. (2018) (their Figure 8), there are a large number of magnetopause crossings with thickness less than 500 km. The thinnest magnetopause in our data set is 43 km.

2.2.3. Magnetopause Current Sheet Density

The highly accurate calibrations of the MMS FPI instruments enable us to calculate the current density directly from plasma moments: $\mathbf{J} = n_e q(\mathbf{V}_i - \mathbf{V}_e)$, where n_e is the electron density, $\mathbf{V}_i$ and $\mathbf{V}_e$ are the electron and ion bulk velocity from the FPI instrument, and q is the elementary charge. In the database, we store both the *average* current across the current sheet thickness, $\mathbf{J_{AVE}}$, as well as the *peak* current, $\mathbf{J_{MAX}}$.

Note that this procedure is different from that used on Cluster and THEMIS data, where an average magnetopause current density across the magnetopause was estimated from the magnetic field and the current sheet thickness using Ampères law. Not surprisingly, the *peak* currents from MMS are usually much higher than the *average* current from THEMIS and Cluster.

2.2.4. Rotational Discontinuities and Reconnection

In Paschmann et al. (2018), the classification of the magnetopause as a tangential discontinuity, or a rotational discontinuity (RD), was based on the Walén test (Walén, 1944), expressed as a jump condition:

$$\Delta\mathbf{V} = \pm\Delta\mathbf{V}_\mathrm{A}, \tag{3}$$

where $\Delta\mathbf{V}$ is the change in velocity between the upstream magnetosheath (at t_{MFRu}) and a location inside the magnetopause which maximizes $\Delta\mathbf{V}$ (at $t_{max\Delta V}$, marked with vertical dashed blue line across Figures 2c to 2d). $\pm\Delta\mathbf{V_A}$ is the corresponding change in Alfvén velocity, corrected for the effect of pressure anisotropy, $\mathbf{V_A} = \mathbf{B}[(1-\alpha)/\mu_0\rho]^{0.5}$ with $\alpha = (p_{\parallel} - p_{\perp})\mu_0/B^2$. The + sign applies if the normal component of the magnetic field and plasma have the same sign, while the − sign applies if they have opposite signs.

For an ideal RD, the two sides of the discontinuity are coupled by the magnetic field and plasma attached to it, allowing transfer of plasma across the discontinuity. At the magnetopause, the magnetic field undergoes

a rotation from the magnetosheath side (which, for the dayside subsolar magnetopause is essentially the orientation of the IMF) to the magnetospheric orientation (typically dominated by the Earth's dipole field). A large increase in plasma velocity occurs so that equation (3) is satisfied. This relation can therefore be used to identify RDs and thus signatures of reconnection.

For an ideal tangential discontinuity, there is no mixing of magnetic field or plasma across the discontinuity. Composition and plasma parameters can be very different between the two regions separated by the discontinuity, and equation (3) does not hold.

Equation (3) may involve both a magnitude and a directional change which both need to be considered to check for reconnection signatures. This requirement led Sonnerup et al. (2018) to work out a single quality index to assess how well the Walén relation was satisfied. Such a simplified quality index, according to (Sonnerup et al., 2018), "..would be more convenient for the presentation of statistical information..." This index is defined as

$$Q^{\pm} = \pm\left(1 - \frac{|\Delta\mathbf{V} \mp \Delta\mathbf{V}_{\mathrm{A}}|}{|\Delta\mathbf{V}| + |\Delta\mathbf{V}_{\mathrm{A}}|}\right). \tag{4}$$

The range of $Q^{\pm}$ is limited to the range $[-1$ to $+1]$. When applied to the outer part of the dayside magnetopause, where inflow from the magnetosheath into the reconnection exhaust jet is expected, the upper sign, Q^{+} applies to regions north of a reconnection site, where the normal flow and field in the magnetopause current sheet have the same direction. Correspondingly, Q^{-} applies to regions south of the reconnection site, where the normal flow and field are oppositely directed. For our purpose, it is irrelevant whether reconnection takes place north or south of the spacecraft, and this is obviously dependent of the spacecraft orbit. In our calculations, we only use the absolute value of Q. Implicitly, we assume a single X line in the vicinity of the spacecraft.

To facilitate comparison with earlier studies, we also perform a "classic" Walén test, in which the measured velocity in the deHoffmann-Teller frame, $\mathbf{V} - \mathbf{V}_{\mathbf{HT}}$, is plotted component by component against the Alfvén velocity, $\mathbf{V}_{\mathbf{A}}$. The resulting linear regression slope between the two velocities—the Walén slope—is stored in the MMS database. The full time interval, from t_{MFRu} to t_{MFRd} is used to determine the Walén slope. For example, Cluster and THEMIS, using the full time interval could be justified and, given the limited time resolution of plasma moments, often the only viable option. For MMS, with its much higher time resolution, Paschmann et al. (2018) pointed out that using the full time interval often gives less meaningful results, so Walén slopes based on shorter time intervals (t_{MFRu} to $t_{max\Delta V}$ and $t_{max\Delta V}$ to t_{MFRd}) were also calculated and stored in the MMS database. These are not directly comparable to the THEMIS and Cluster results, however.

The high time resolution of the FPI plasma moments enable us to detect other reconnection signatures such as high speed jetting (fast plasma flow from the reconnection exhaust) or large peak currents directly. In addition to the above described $\Delta\mathbf{V}$, the absolute maximum flow velocity, V_{MAX} is also stored the MMS current sheet database. At the dayside, where the background (magnetosheath) flow is stagnant and turbulent, signatures of reconnection associated jetting often appear as distinct velocity enhancements. At the flanks, however, the magnetosheath flow speed can be significant, and often comparable to the local Alfvén velocity. Organizing our collection of crossings by the stored V_{MAX} values therefore does not give any consistent view on how jetting varies between dayside and flanks of the magnetopause.

In the example shown in Figure 2, the Q value is 0.67, and the classic Walén test gives a value of 0.47. A jetting signature, albeit not very pronounced, is also apparent in the V_L component shown in Figure 2c.

2.3. Selection Criteria for Magnetopause Parameters

At the time of writing, the updated MMS current sheet database contains 6,194 observations of current sheets classified as magnetopauses (details about the classification are given in Appendix A). Not all of these events are suitable for our purpose; Some crossings are incomplete or fail to meet the MFR eigenvalue criteria. We have only selected events flagged as "complete" in the updated Paschmann et al. (2018) database, with the additional requirement that the ratio between the intermediate and smallest eigenvalue from the MFR analysis, λ_2/λ_1, is 2 or above. Figure 2 shows an example of a "complete" crossing, that is, the entire magnetopause crossing takes place within the time interval where burst mode data is available, and the spacecraft traverses the entire magnetopause current sheet.

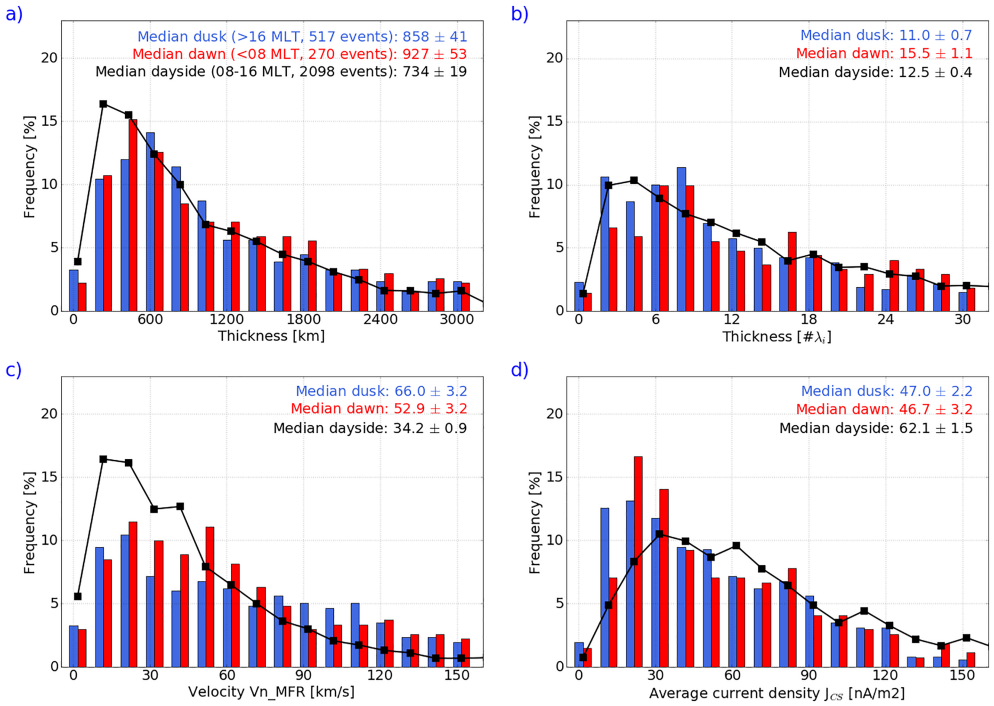

Figure 3. (a) Histograms of the thickness in units of kilometers for the dawn and dusk magnetopause flanks. The black line shows the corresponding distributions from the dayside magnetopause. (b) Same as panel (a), but thickness in units of ion gyroradii. (c) Histogram of magnetopause normal velocities. (d) Histogram of average current density. Values along the abcissae indicate the lower value of a histogram bin; for example, the first bin in panel (a) indicates the frequency of values in the range 0 to 200 km. Values given in each panel are median values and their standard errors for each sector.

After filtering out unsuitable crossings, we are left with a total of 2,885 magnetopause crossings across all dayside local time sectors. Using our definition of *dawn*, *dayside*, and *dusk* as MLT locations < 08, 08–16, and > 16, illustrated in Figure 1, there are 270 dawn crossings, 2,098 dayside crossings, and 517 dusk crossings (there is one extra dusk crossing season, thus the higher number of dusk crossings), included in the MMS current sheet database at the time of writing.

3. Results

We first focus on key parameters for the regions *dawn*, *dayside*, and *dusk*. This enables a direct comparison to the earlier Cluster and THEMIS results. In section 3.3, we then utilize the large number of MMS magnetopause crossings and a finer division into MLT sectors to see how the key parameters change across local times from dawn to dusk.

3.1. Macroscopic Magnetopause Parameters at Dawn, Dayside, and Dusk

Figure 3 shows the distributions of some of the key macroscopic magnetopause parameters using the division into dawn (red color), dusk (blue) and dayside (black) as illustrated in Figure 1. Most of the distributions have κ like shapes with a high value tail. Moments of the distributions and some of the key upstream parameters and the solar wind, IMF and Dst values are also summarized in Table 1. Uncertainties listed in Table 1 are standard errors, δ, calculated from the number of samples within the region, N, and the standard deviation, σ of the distribution; $\delta = \sigma/\sqrt{N}$.

External conditions such as the solar wind dynamic pressure, IMF, and geomagnetic disturbance indices are also stored in the database. These are calculated from the OMNI data set (King & Papitashvili, 2005), and are fairly similar for the three regions. We note, however, that the solar wind dynamic pressure is approximately twice as high as in the THEMIS study in Haaland et al. (2019) and also higher than the dayside MMS study of Paschmann et al. (2018) (median values in these studies were in the range 1.3–1.9 nPa).

Table 1
Key Magnetopause Parameters From the Updated MMS Database of Paschmann et al. (2018) (Rows 1–7), With Upstream Conditions (Rows 8–10) and Corresponding Median Solar Wind, IMF, and Dst Values (Rows 11–14)

	Parameter	Dawn	Dusk	Dayside (08–16 MLT)
1	N = Number of crossings	270	517	2,098
2	Thickness (km)	927±53	858±41	734±19
3	Thickness (λ_i)	15.5	11.0	12.5
4	Thickness (R_{gi})	8.1	7.8	7.3
5	Vn_{MFR} (km/s)	52.9±3.2	66.0±3.2	34.2±0.9
6	Vn_{HT} (km/s)	49.1±3.0	72.4±3.2	34.7±1.0
7	Current density (nA/m^2)	46.7±3.2	47.0±2.2	62.1±1.5
8	n (cm^{-3})	15.2±0.8	9.2±0.4	14.9±0.3
9	$T_{i\perp}$ (eV)	234±18	474.1±48	360±8
10	$\|B\|$ (nT)	25.2±0.8	31.1±0.6	30.3±0.4
11	By IMF (nT)	1.0	2.1	1.1
12	Bz IMF (nT)	−0.1	−0.1	−0.0
13	Pdyn (nPa)	2.6	3.2	2.7
14	Dst index (nT)	−10	−17	−13

Note. Uncertainties given are standard errors, $\delta = \sigma/\sqrt{N}$, where σ is the standard deviation and N is the number of events.

Figure 3a shows the distribution of magnetopause thicknesses in units of kilometers. Dawn and dusk distributions are very similar, with the median dawn magnetopause thickness marginally larger than at dusk. Dayside values are shifted toward smaller values, indicating a thinner dayside magnetopause.

Figure 3b shows the thickness normalized to the upstream ion inertial length (see equation (1)). These values suggest a more significant dawn-dusk asymmetry with a higher number of thinner magnetopauses at dusk. Scaling to the ion gyroradius (not shown in Figure, but averages listed in the fourth row of Table 1), determined from the upstream ion temperature and magnetic field (ninth and tenth rows in Table 1) showsasimilar distribution.

Figure 3c shows the distributions of magnetopause normal velocities. In contrast to the earlier Cluster and THEMIS studies (Haaland et al., 2014, 2019), average dusk velocities are higher than at dawn in the MMS data set. Dayside velocities are significantly lower. As seen in Table 1 this result holds also if we use the velocity from the HT analysis rather than the MFR analysis.

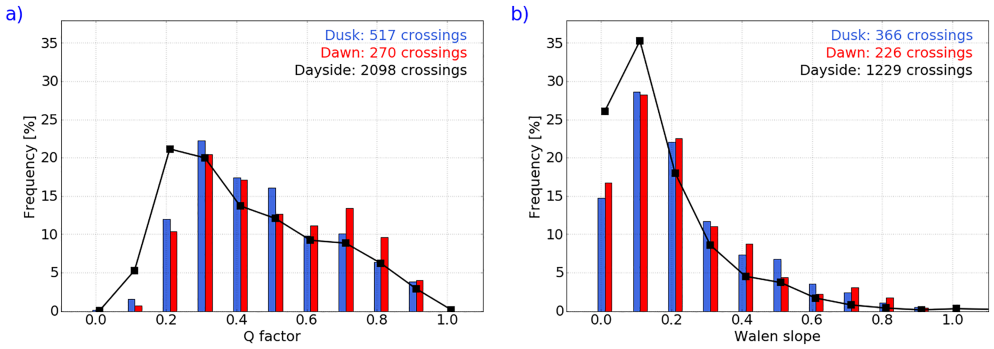

Figure 4. (a) Histograms of the Sonnerup et al. (2018) Q index of Alfvénicity. (b) Histograms of the Walén slopes. Color coding and symbols are as in Figure 3, but there are fewer events in (b) since the Walén slope is only calculated for events with well-determined de-Hoffmann-Teller frames.

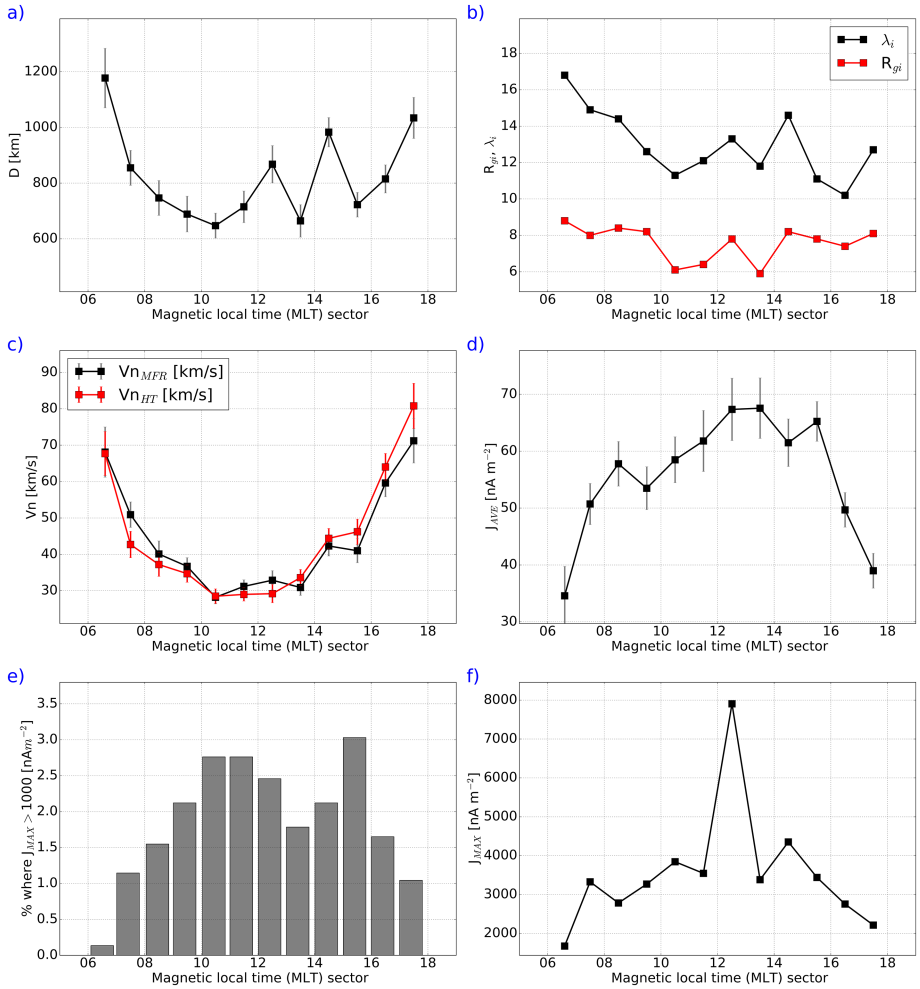

Figure 5. MLT profiles of key parameters across the dayside magnetopause. Each of the top four panels shows a key parameter (and standard error, where applicable) as a function of MLT sector. (a) Absolute thickness in units of kilometers. (b) Thickness normalized to the upstream ion inertial length (black lines and symbols) and upstream ion gyroradius (red), respectively. (c) Magetopause normal velocity based on MFR (black) and HT/MVAB0 (red) analyses. (d) Average current density across the full current sheet, based on FPI ion and electron moments. (e) Percentage of crossings with J_{MAX} > 1,000 nA m^{-2} within each MLT sector. (f) Peak current density, J_{MAX} within each MLT sector.

Figure 3d shows the distribution of current densities (average current density across the current sheet). Once again, there is very little difference between dawn and dusk, but the average current density at the flanks are significantly lower than at the dayside, consistent with THEMIS results. (A comparison to Cluster is not possible, since it did not traverse the low latitude dayside magnetopause).

3.2. Reconnection Signatures

Figure 4a shows the distributions of the Sonnerup et al. (2018) *Q* factor—a measure of the level of Alfvénicity of the flow in the outer layer of the magnetopause, described in section 2.2.4. Recall that a *Q* factor of 1 means perfect Alfvénicity (both change in flow magnitude and flow direction follows the change in Alfvén velocity) and would indicate the presence of an RD associated with reconnection. We note that most of the crossings have *Q* values below 0.5.

For comparison with the Cluster and THEMIS based dawn-dusk studies, we also show the "classic" Walén slope distribution in Figure 4b. Only values from crossings with a well defined HT frame (HT correlation coefficient ≥ 0.85) are shown. In the Cluster and THEMIS studies, and also earlier studies by, for example, Chou and Hau (2012); Paschmann et al. (2005), crossings with Walén slope ≥ 0.5 were classified as RDs. Comparing the two panels, and using a Walén slope, respectively a *Q* value of 0.5 as a threshold, one observes that the *Q* factor has a flatter distribution and a larger fraction of cases indicating RDs.

Table 2
Similar to Table 1, but With a Finer, 1 hr MLT Resolution to Show How the Parameters Vary Across the Local Time Sectors

A	B	C	D	E	F	G	H	I	J	K	L
		Thickness			Speed		Current density		Upstream values		
MLT	N	d	$\#R_g$	$\#\lambda_i$	Vn_{MFR}	Vn_{HT}	J_{AVE}	J_{MAX}	N_i	$T_{i\perp}$	$\lvert B\rvert$
		(km)			(km/s)		(nA/m^2)		(cm^{-3})	(eV)	(nT)
06–07	83	1149	8.8	16.8	59	64	37	2,237	13.0	214	24.1
07–08	186	833	8.0	14.9	51	43	51	3,328	16.3	236	25.4
08–09	182	747	8.4	14.4	42	38	58	2,783	16.4	275	29.5
09–10	223	641	8.2	12.6	37	37	54	3,269	18.0	309	33.9
10–11	269	664	6.1	11.3	29	28	59	3,844	15.3	370	29.9
11–12	253	682	6.4	12.1	30	27	65	5,448	15.8	399	30.6
12–13	235	783	7.8	13.3	31	26	66	7,904	14.3	421	30.1
13–14	250	651	5.9	11.8	29	33	67	4,045	15.0	336	29.4
14–15	352	944	8.2	14.6	41	45	61	4,352	13.5	379	28.6
15–16	334	722	7.8	11.1	41	46	65	3,440	13.4	381	31.0
16–17	317	827	7.4	10.2	59	64	50	2,755	9.2	527	33.5
17–18	199	1024	8.1	12.7	78	84	38	2,215	9.1	431	25.0

Note. The columns show the following: A = magnetic local time sector; B = number of observations within sector; C = magnetopause thickness in units of kilometers; D = thickness in units of ion gyroradii; E = thickness in units of ion inertial lengths; F = magnetopause speed derived from MFR analysis; G = magnetopause speed derived from HT analysis; H = average current density across the current sheet; I = peak current density within local time sector; J = upstream ion density; K = upstream ion perpendicular temperature and L = upstream *B* field.

The use of the *Q* factor and the Walén slope as reconnection indicators, as well as discrepancies between the two parameters will be investigated further and addressed in a separate publication.

3.3. The Magnetopause in Different MLT Sectors

The large number of magnetopause crossings allows for an even finer local time division than possible with the Cluster and THEMIS data sets. In Figure 5, we have divided the dayside sector into smaller, 1 hr magnetic local time (MLT) sectors and calculated averages (medians) and their standard errors (where applicable). When interpreting these values, one should have in mind that there may be a seasonal dependence; dawn is covered in the Northern Hemisphere spring season (starting in February), dayside during summer and dusk toward autumn (most duskward observations are around October). Dipole tilt should be fairly similar for the dawn and dusk data sets, though. Table 2 shows the corresponding details, where each row shows key values for a particular local time sector.

From Figure 5 and Table 2, we can infer a transition from a rather thick, dynamic magnetopause at dawn toward a thinner and more rigid magnetopause with higher current densities at the subsolar point, and back to a thicker, more dynamic magnetopause at dusk. The dawn sector shows a thicker and less dynamic magnetopause (lower normal velocities) than at dusk, but the dawn-dusk asymmetry is not very pronounced.

As already noted in Paschmann et al. (2018), the MMS current sheet database contains a number of crossings where the peak current density exceeds 1,000 nA^{-2}. Magnetopause with large peak currents are candidates for electron diffusion region encounters (Burch et al., 2016), and thus reconnection. As shown in Figures 5e and 5f, peak currents are significantly higher than average currents, and highest and most frequent around noon.

4. Discussion

In terms of magnetopause thickness, the dayside median value, 734 km (corresponding to 12.5 λ_i), is very similar to earlier results reported by Berchem and Russell (1982), Phan and Paschmann (1996), Paschmann et al. (2018), and Haaland et al. (2019). Absolute thicknesses (in units of kilometers) at the flanks are approximately 15–20% thicker than at the dayside, but unlike the earlier THEMIS and Cluster results, the dawn-dusk

asymmetry is less pronounced. Consistent with the Cluster and THEMIS dawn-dusk studies, there is a more pronounced dawn-dusk asymmetry in thickness when normalized to the ion inertial length.

Some of the asymmetry can be explained by upstream (magnetosheath) conditions. As noted from Table 1, the magnetosheath at dawn is characterized by a higher plasma density, lower magnetic field, and lower temperature than at dusk. In our data set, the corresponding dayside upstream conditions fall in between those of the dawn and dusk. The asymmetry between dawn and dusk upstream conditions has already been noted by several studies (Dimmock et al., 2016, 2017; Němeček et al., 2002; Paularena et al., 2001; Walsh et al., 2012) and often attributed to kinetic effects in the interaction between the [predominantly Parker spiral like] IMF with the Earth's bow shock. Compared to the earlier THEMIS and Cluster studies, the MMS collection of magnetopause observations is also characterized by higher solar wind dynamic pressures.

The characteristic normal velocities at dawn and dusk are somewhat surprising. In contrast to the Cluster and THEMIS results, the MMS results indicate that the dusk magnetopause is more dynamic than at dawn. Strong motion at the flanks have often been taken to be the result of enhanced Kelvin-Helmholtz wave activity set up by flow shears (Eriksson et al., 2016; Nykyri, 2013; Taylor et al., 2012). It is still debated whether this activity is more pronounced at dawn or dusk.

The magnetopause current density, characterized by the average current density, is almost twice as high near noon compared to the flanks. There is no significant dawn-dusk asymmetry in the average current density. The highest peak currents (indicative of diffusion region encounters) are also found near noon. Once again, there is no significant difference between dawn and dusk flanks.

From a model perspective one would expect the highest reconnection occurence where the magnetic shear (angle between upstream and downstream B field) maximizes (Trattner et al., 2017). Our data set does not show any significant MLT dependence on shear angle. Neither the average shear angle (around 80–90°, consistent with the average ± By dominated IMF) nor the maximum shear angle ($\geq$ 172° in all MLT sectors) show any strong MLT variation.

5. Summary and Conclusion

We have used a large data set of MMS magnetopause observations to characterize the flank magnetopause, and to compare the dayside and flank magnetopause. The methodology and classifications of the events studied are identical to those in Paschmann et al. (2018), but the data set has been extended all burst mode intervals from MMS Phase II (after 2017, apogee was raised to 25 Re).

The results, based on almost 3,000 MMS magnetopause crossings, are summarized as follows:

- The flank magnetopause is thicker than the dayside magnetopause. This applies both to the absolute thickness in units of kilometers and normalized to the upstream ion gyroradius or upstream ion inertial length.
- Expressed in units of ion inertial lengths, the dawn flank magnetopause current sheet is on average thicker than at dusk.
- The average current density is higher at the dayside magnetopause, and it is almost twice as high as the average current density at the flanks. There is no significant dawn-dusk asymmetry in current density.
- The highest peak currents, indicative of diffusion region encounters, are found near noon.
- The flank magnetopause have a higher average normal velcity than at the dayside. The highest normal velocities are found at the dusk flank.

Appendix A: Classification of MMS Burst Mode Data

Most of the burst mode events in the updated Paschmann et al. (2018) MMS database have been classified and given a set of seven flags describing the nature of the current sheet. The flags and their meaning were defined after discussion between the lead authors of this paper in consultation with the members of ISSI team 442 set up to explore the MMS current sheet database.

The event classification is based on *visual inspection* of summary plots of ion moments and spectra similar to Figure 2 and corresponding plots for electrons, with 2-hr MMS quicklook plots and IMF information providing the context. A special software tool displaying this information in one screen along with checkboxes to

register the events in the database was developed for this purpose. The seven flags and their possible values are the following:

1. *Crossing type*; One of *mp* (magnetopause), *bs* (bow shock), *msh* (magnetosheath), *sp* (magnetosphere), *sw* (solar wind), *ot* (other, unknown).
2. *Crossing direction*; *i* (inbound), *o* (outbound), *udef* (undefined).
3. B_L profile; *mono* (monotonic), *nmon* (nonmonotonic), *udef* (undefined).
4. *Fit quality*; *gf* (good fit), *mf* (mediocre fit), *bf* (bad fit).
5. *Number of crossings* within burst interval; *sing* (single crossing), *multi* (multiple crossings present).
6. *Crossing completeness*; *comp* (complete crossing), *part* (partial crossing), *over* (several overlapping crossings), *harr* ("clean" Harris sheet like crossing).
7. *Event qualification*; *keep* (keep event), *excl* (exclude event for some reason), *intr* (particularly interesting event, flag for later investigation).

The *inbound/outbound flag* is only relevant for *mp* and *bs*; for the others *i* and *o* are meaningless and are therefore set to *udef*. For *sp*, *sw*, *msh* and *ot* events, flags 3–6 above are less important or less meaningful, and therefore often not set, or left to the default values (*udef,bad,multi,part*).

The B_L *profile*, relevant for magnetopauses and bow shock crossings, describes how B_L changes from upstream to downstream (or vice versa); a nonmonotonic change would indicate the presence of internal structures or back-and-forth motion of the current sheet.

Fit quality loosely describes how well the B_L profile fits a one-dimensional current sheet model.

Crossing completeness is meant to describe whether the burst mode interval encompasses the full current sheet, just parts of it, or overlaps with another event in the database. An event flagged as partial can mean one of three things: (1) *mp* or *bs* crossing not fully contained within the burst event, that is, appears to extend to earlier or later times; this occurs relatively seldom, but was the original definition. (2) The full *mp* or *bs* crossing occurs in burst interval, but is not caught by the search routine, that is, not between the red/green lines in Figure 2 for some reason. (3) The spacecraft enters a magnetopause boundary layer from the magnetosphere, but does not actually cross into the magnetosheath; this occurs quite frequently.

If the current sheet crossing is complete and has a very clean, Harris sheet like profile in B_L, captured within the burst interval, the completeness of the event is classified as *harr*. (In retrospect, one could argue that this classification should have been a B_L profile flag instead).

The last flag, *event qualification*, was introduced to bookmark particular interesting events worth a closer examination (flagged *intr*), or to discard obvious erronous events, for example, large data gaps, obvious misidentifications. For the moment, the large majority is simply flagged *keep*, but this may change as we start investigating events more closely.

Using a Structured Query Language (SQL) to select events from the database, this flag information enables us to search for particular current sheet properties. For the characterization of the magnetopause in this paper, we only include current sheets flagged as complete magnetopause crossings: "*mp,comp*" but do not require them to have clean, Harris sheet B_L profiles.

Acknowledgments
Research efforts by S. H. were supported by the Norwegian Research Council under Grant 223252. Research by J. P. E was supported by UKRI/STFC Grant ST/S000364/1. Research at Southwest Research Institute is supported by a MMS prime contract from NASA. Research at UC Berkeley is supported by NASA grants NNX17AE12G and 80NSSC18K1380. VC acknowledges support from ESA project MAGICS, PRODEX contract C4000127660. The authors are grateful to the International Space Science Institute, Bern, Switzerland, for the support of ISSI team 442—Study of the Physical Processes in Magnetopause and Magnetosheath Current Sheets Using a Large MMS Database. Calculations in this paper have made use of the QSAS science analysis system, provided by Imperial College, London. All MMS data are publicly available (through the following: https://lasp.colorado.edu/mms/sdc/public/).

References

Berchem, J., & Russell, C. T. (1982). The thickness of the magnetopause current layer—ISEE 1 and 2 observations. *Journal Geophysical Research*, *87*, 2108–2114. https://doi.org/10.1029/JA087iA04p02108

Burch, J. L, Moore, T. E, Torbert, R. B., & Giles, B. L. (2016). Magnetospheric Multiscale overview and science objectives. *Space Science Reviews*, *199*, 5–21. https://doi.org/10.1007/s11214-015-0164-9

Chou, Y. C., & Hau, L. N. (2012). A statistical study of magnetopause structures: Tangential versus rotational discontinuities. *Journal of Geophysical Research*, *117*, A08232. https://doi.org/10.1029/2011JA017155

Dimmock, A. P, Osmane, A, Pulkkinen, T. I, Nykyri, K., & Kilpua, E. (2017). Temperature variations in the dayside magnetosheath and their dependence on ion-scale magnetic structures: THEMIS statistics and measurements by MMS. *Journal of Geophysical Research: Space Physics*, *122*, 6165–6184. https://doi.org/10.1002/2016JA023729

Dimmock, A. P, Pulkkinen, T. I, Osmane, A., & Nykyri, K. (2016). The dawn-dusk asymmetry of ion density in the dayside magnetosheath and its annual variability measured by THEMIS. *Annales Geophysicae*, *34*, 511–528. https://doi.org/10.5194/angeo-34-511-2016

Eriksson, S, Lavraud, B, Wilder, F. D, Stawarz, J. E, Giles, B. L, Burch, J. L., & Goodrich, K. A. (2016). Magnetospheric Multiscale observations of magnetic reconnection associated with Kelvin-Helmholtz waves. *Geophysical Research Letters*, *43*, 5606–5615. https://doi.org/10.1002/2016GL068783

Haaland, S, Reistad, J, Tenfjord, P, Gjerloev, J, Maes, L, DeKeyser, J., & Dorville, N. (2014). Characteristics of the flank magnetopause: Cluster observations. *Journal of Geophysical Research: Space Physics*, *119*, 9019–9037. https://doi.org/10.1002/2014JA020539

Haaland, S, Runov, A, Artemyev, A., & Angelopoulos, V. (2019). Characteristics of the flank magnetopause: THEMIS observations. *Journal of Geophysical Research: Space Physics*, *124*, 3421–3435. https://doi.org/10.1029/2019JA026459

Harris, E. G. (1962). On the plasma sheath separating regions of oppositely directed magnetic field. *Nuovo Cimento*, *23*, 115–121.

Hasegawa, H. (2012). Structure and dynamics of the magnetopause and its boundary layers. *Monographs on Environment, Earth and Planets*, *1*, 71–119. https://doi.org/10.5047/meep.2012.00102.0071

Khrabrov, A. V., & Sonnerup, B. U. Ö. (1998a). deHoffmann-Teller analysis. In *Analysis methods for multi-spacecraft data* (pp. 221). Noordwijk: ESA Publications Division.

Khrabrov, A. V., & Sonnerup, B. U. Ö. (1998b). Orientation and motion of current layers: Minimization of the Faraday residue. *Geophysical Research Letters*, *25*, 2373.

King, J. H., & Papitashvili, N. E. (2005). Solar wind spatial scales in and comparisons of hourly Wind and ACE plasma and magnetic field data. *Journal of Geophysical Research*, *110*, A02104. https://doi.org/10.1029/2004JA010649

Lavraud, B, Zhang, Y. C, Vernisse, Y, Gershman, D. J, Dorelli, J, Cassak, P. A., & Yokota, S. (2016). Currents and associated electron scattering and bouncing near the diffusion region at Earth's magnetopause. *Geophysical Research Letters*, *43*, 3042–3050. https://doi.org/10.1002/2016GL068359

Němeček, Z., Šafránková, J., Zastenker, G. N., Pišoft, P., & Paularena, K. I. (2002). Spatial distribution of the magnetosheath ion flux. *Advances in Space Research*, *30*, 2751–2756. https://doi.org/10.1016/S0273-1177(02)80402-1

Nykyri, K. (2013). Impact of MHD shock physics on magnetosheath asymmetry and Kelvin-Helmholtz instability. *Journal of Geophysical Research*, *118*, 5068–5081. https://doi.org/10.1002/jgra.50499

Paschmann, G, Haaland, S. E, Phan, T. D, Sonnerup, B. U. Ö., Burch, J. L., Torbert, R. B., & Fuselier, S. A. (2018). Large-scale survey of the structure of the dayside magnetopause by MMS. *Journal of Geophysical Research: Space Physics*, *123*, 2018–2033. https://doi.org/10.1002/2017JA025121

Paschmann, G, Haaland, S, Sonnerup, B. U. Ö., Hasegawa, H., Georgescu, E., Klecker, B., & Vaivads, A. (2005). Characteristics of the near-tail dawn magnetopause and boundary layer. *Annales Geophysicae*, *23*, 1481.

Paschmann, G., & Sonnerup, B. U. O. (2008). Proper frame determination and Walen test. *ISSI Scientific Reports Series*, *8*, 65–74.

Paularena, K. I, Richardson, J. D, Kolpak, M. A, Jackson, C. R., & Siscoe, G. L. (2001). A dawn-dusk density asymmetry in Earth's magnetosheath. *Journal of Geophysical Research*, *106*, 25,377–25,394. https://doi.org/10.1029/2000JA000177

Phan, T. D, Eastwood, J. P, Cassak, P. A, Øieroset, M., Gosling, J. T., Gershman, D. J., & Wilder, F. D. (2016). MMS observations of electron-scale filamentary currents in the reconnection exhaust and near the X line. *Geophysical Research Letters*, *43*, 6060–6069. https://doi.org/10.1002/2016GL069212

Phan, T. D., & Paschmann, G. (1996). Low-latitude dayside magnetopause and boundary layer for high magnetic shear 1. Structure and motion. *Journal of Geophysical Research*, *101*(10), 7801–7816.

Pollock, C., Moore, T., Jacques, A., Burch, J., Gliese, U., Saito, Y., & Zeuch, M. (2016). Fast plasma investigation for Magnetospheric Multiscale. *Space Science Reviews*, *199*, 331–406. https://doi.org/10.1007/s11214-016-0245-4

Russell, C. T, Anderson, B. J, Baumjohann, W, Bromund, K. R, Dearborn, D, Fischer, D., & Richter, I. (2016). The Magnetospheric Multiscale Magnetometers. *Space Science Reviews*, *199*, 189–256. https://doi.org/10.1007/s11214-014-0057-3

Sonnerup, B. U, Haaland, S. E., & Paschmann, G. (2008). Discontinuity orientation, motion, and thickness. *ISSI Scientific Reports Series*, *8*, 1–16.

Sonnerup, B, Haaland, S., Paschmann, G., & Denton, R. (2018). Quality measure for the Walén relation. *Journal of Geophysical Research: Space Physics*, *123*, 9979–9990. https://doi.org/10.1029/2018JA025677.

Sonnerup, B. U. Ö., & Scheible, M. (1998). Minimum and maximum variance analysis, *Analysis methods for multi-spacecraft data* (pp. 1850). Noordwijk: ESA Publications Division.

Taylor, M. G. G. T., Hasegawa, H., Lavraud, B, Phan, T., Escoubet, C. P., Dunlop, M. W., & Wild, J. A. (2012). Spatial distribution of rolled up Kelvin-Helmholtz vortices at Earth's dayside and flank magnetopause. *Annales Geophysicae*, *30*, 1025–1035. https://doi.org/10.5194/angeo-30-1025-2012

Terasawa, T., Kawano, H, Shinohara, I, Mukai, T, Saito, Y, Hoshino, M., & Kokubun, S. (1996). On the determination of a moving MHD structure: Minimization of the residue of integrated Faraday's equation. *Earth, Planets and Space*, *48*, 603.

Trattner, K. J, Burch, J. L, Ergun, R, Eriksson, S, Fuselier, S. A, Giles, B. L., & Wilder, F. D. (2017). The MMS dayside magnetic reconnection locations during Phase 1 and their relation to the predictions of the Maximum Magnetic Shear Model. *Journal of Geophysical Research: Space Physics*, *122*, 11,991–12,005. https://doi.org/10.1002/2017JA024488

Walén, C. (1944). On the theory of sunspots. *Arkiv för matematik, astronomi och fysik*, *30*, 1–87.

Walsh, B. M, Sibeck, D. G, Wang, Y., & Fairfield, D. H. (2012). Dawn-dusk asymmetries in the Earth's magnetosheath. *Journal of Geophysical Research*, *117*, 12211. https://doi.org/10.1029/2012JA018240

Young, D. T., Burch, J. L., Gomez, R. G., De Los Santos, A., Miller, G. P, Wilson, P., & Webster, J. M. (2016). Hot plasma composition analyzer for the Magnetospheric Multiscale mission. *Space Science Reviews*, *199*, 407–470. https://doi.org/10.1007/s11214-014-0119-6